Check for updates

JGR Solid Earth

RESEARCH ARTICLE
10.1029/2023JB028090

Lower-Crustal Normal Faulting and Lithosphere Rheology in the Atlas Foreland

Sam Wimpenny[1,2], **Tim Craig**[1], **and Alice Blackwell**[1]

[1]COMET, School of Earth and Environment, University of Leeds, Leeds, UK, [2]COMET, School of Earth Sciences, University of Bristol, Bristol, UK

Key Points:

- We report a 31 km-deep normal-faulting earthquake in the foreland of the Algerian Atlas
- To account for the gravity anomalies and earthquake depth the lithosphere needs to support elastic stresses 5–10 km below the Moho
- Differences in the depth of extension in the Atlas, Andean and Tibetan forelands are explained by different in-plane compressional forces

Supporting Information:

Supporting Information may be found in the online version of this article.

Correspondence to:

S. Wimpenny,
s.wimpenny@bristol.ac.uk

Citation:

Wimpenny, S., Craig, T., & Blackwell, A. (2023). Lower-crustal normal faulting and lithosphere rheology in the Atlas foreland. *Journal of Geophysical Research: Solid Earth*, *128*, e2023JB028090. https://doi.org/10.1029/2023JB028090

Received 17 OCT 2023
Accepted 11 DEC 2023

Author Contributions:

Conceptualization: Sam Wimpenny, Tim Craig
Formal analysis: Sam Wimpenny
Methodology: Sam Wimpenny, Tim Craig, Alice Blackwell
Software: Sam Wimpenny, Alice Blackwell
Visualization: Sam Wimpenny
Writing – original draft: Sam Wimpenny
Writing – review & editing: Tim Craig, Alice Blackwell

© 2023. The Authors.
This is an open access article under the terms of the Creative Commons Attribution License, which permits use, distribution and reproduction in any medium, provided the original work is properly cited.

Abstract Earthquakes beneath the foreland basins of the Andes and Tibet are rare but follow a simple pattern, with normal faulting from 0 to 20 km depth and reverse-faulting from 30 to 50 km depth. The switch in faulting style with depth suggests that the stresses generated by foreland flexure are large enough to break faults, with opposite senses of horizontal strain either side of a neutral surface in the mid-crust. In this study, we document a 31 km-deep M_w 5.2 normal-faulting earthquake in the forelands of the Algerian Atlas Mountains near Biskra. The Biskra earthquake is of interest, as it indicates that the lower crust of the Atlas forelands is in extension at the same depth that the Tibetan and Andean forelands are in compression. In order to match the gravity anomalies and the depth of normal faulting near Biskra, we find that models of lithospheric flexure require the neutral surface to be >35 km deep and at least the top 5–10 km of the lithospheric mantle supports elastic bending stresses. The differences in the pattern of earthquakes between the forelands of Tibet, the Andes and the Algerian Atlas can be explained by differences in the buoyancy forces acting between these mountain ranges and their lowlands that place the forelands into varying amounts of net compression. Our results suggest the upper mantle beneath cratonic foreland lithosphere may therefore support bending stresses of the order of 10s of MPa, likely because it is cool and the strain rates associated with bending are low.

Plain Language Summary The strong part of Earth's outer layer bends like a plate along the margins of mountain ranges. The stresses created by this bending can break faults in earthquakes, leading to a characteristic pattern of shallow extensional faulting overlying deeper compressional faulting. Here we document a new example of bending-related extensional faulting along the southern margin of the Atlas Mountains in Algeria, which indicates that the switch from extension to compression is about 5–10 km deeper in this setting when compared with the more well-known examples from Tibet and the Andes. In order to explain the depth of extensional faulting, and the shape of the bending plate in the region, we find that North African plate must support elastic bending stresses within at least the top 10 km of the continental upper mantle. We also find that the lower horizontal compression that the Atlas applies to its edges when compared to higher mountain ranges like the Andes and Tibet can explain the differences in the depth of extensional and compressional faulting between these settings.

1. Introduction

Bending of the foreland lithosphere along the margins of mountain ranges sets up differential stresses that are supported over geological timescales (~10^6 yr) by resistance to deformation. It is generally agreed that within the cratonic lithosphere surrounding high mountain ranges like the Andes and Tibet the stresses generated by bending are supported in a single, strong layer underlain by a weaker layer (Jackson, 2002; Watts & Burov, 2003). However, different estimates for the effective elastic thickness T_e of foreland lithosphere—a proxy for its integrated strength (Burov & Diament, 1995)—have led to different models for the thickness of the strong layer and the bending stresses within it (see Jackson et al., 2008). Some estimates of T_e are similar to, or less than, the thickness of the crust and the depth of foreland seismicity (20–50 km) (e.g., McKenzie & Fairhead, 1997). These observations suggest that the strong layer is ~20–50 km-thick corresponding roughly to the crust, and imply that bending stresses are everywhere close to the yield strength of the lithosphere apart from within a thin (<10 km) elastic core (Jackson, 2002). Alternatively, some estimates of T_e are >60–80 km (e.g., Watts et al., 1995), which suggest that bending stresses are supported over a >60 km-thick layer that extends well into the lithospheric mantle, and would require that the bending stresses are mostly far below the lithosphere's yield strength (Watts & Burov, 2003). A key difference between these two models lies in whether the continental lithospheric mantle is, or is not, strong enough to support significant (i.e., 10s of MPa) bending stresses.

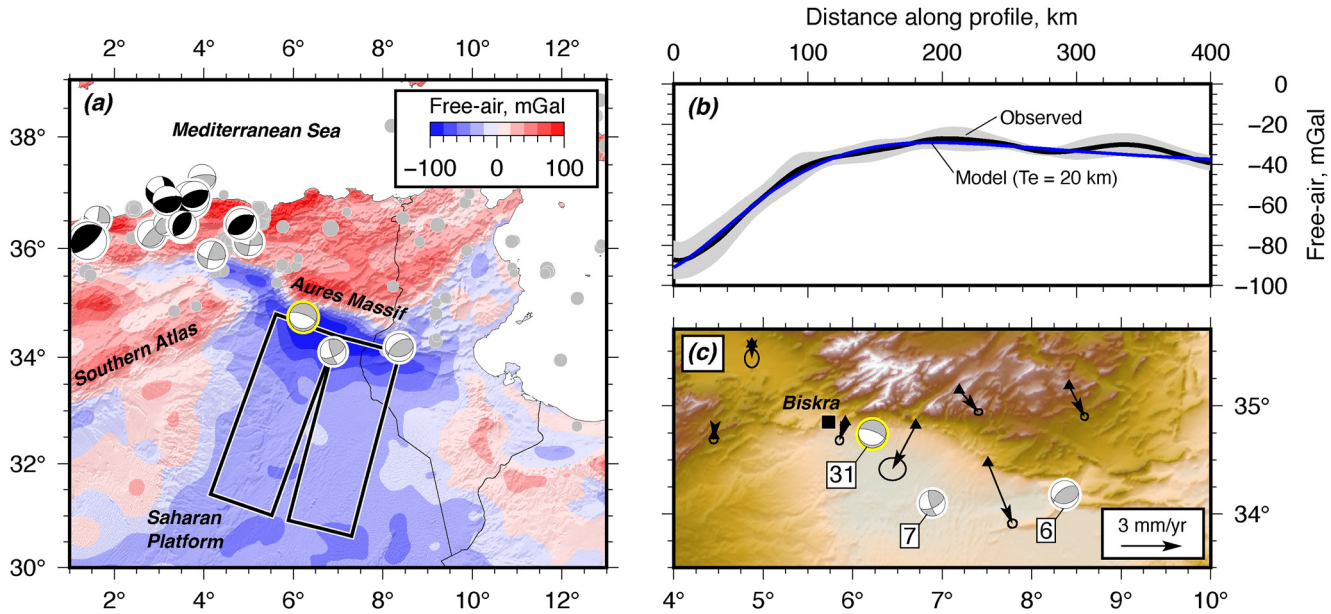

Figure 1. Overview of the 2016 Biskra earthquake. (a) Free-air gravity anomaly map derived from the EIGEN-6C gravity field (Shako et al., 2014) after applying an elliptical filter to remove signals with wavelength <50 km. Focal mechanisms in black have been derived using long-period body-waveform modeling techniques and mechanisms in gray have been derived by matching the vertical-component broadband seismograms with synthetic waveforms (Wimpenny & Watson, 2020). Light gray circles are earthquakes with $m_b \geq 3.0$ taken from the ISC catalog. The 2016 Biskra earthquake is highlighted in yellow. (b) Stacked profile of the free-air gravity anomalies south of the Aurès Massif taken from the black boxes in (a). A model gravity profile for an elastic plate with thickness T_e of 20 km is shown for reference. (c) Geomorphology around the Biskra earthquake. GPS velocity vectors are taken from Bougrine et al. (2019) and are shown relative to stable Nubia. Numbers next to each focal mechanisms show the earthquake centroid depth in kilometers derived from waveform modeling.

An important observation in this debate is that a small number of well-recorded $M_w > 5$ normal-faulting earthquakes with nodal planes parallel to mountain range fronts have been observed between the surface and 20 km depth in the forelands of Tibet and the Andes (e.g., Baranowski et al., 1984; Priestley et al., 2008; Wimpenny, 2022). Reverse-faulting earthquakes are also observed in the same regions, but with centroid depths of 30–50 km in the lower crust and potentially the upper-most few kilometers of the lithospheric mantle (e.g., Priestley et al., 2008; Devlin et al., 2012). The same pattern of extensional earthquakes at 0–30 km depth overlaying compressional earthquakes at 35–50 km depth is observed globally within oceanic lithosphere as it bends at the outer-trench slope adjacent to subduction zones (Chapple & Forsyth, 1979; Craig et al., 2014). In both the oceans and continents, the switch from a single layer of extensional earthquakes to a single layer of compressional earthquakes with depth has been interpreted to reflect the release of elastic stresses generated by bending strains in a single strong layer, with a "neutral surface" lying in between the seismogenic portions of the lithosphere where the bending strains are small (Chapple & Forsyth, 1979; Jackson, 2002).

The neutral surface depth within the forelands of Tibet is 20–25 km, roughly in the middle of the crust. Jackson (2002) argued that the simplest interpretation of this observation is that the majority of the strength of the foreland lithosphere bounding Tibet lies within the seismogenic crust, and that the aseismic upper mantle supports little stress as it deforms through temperature-controlled crystal-plastic creep. However, it is also possible that the neutral surface could be shifted shallower than the middle of the strong layer due to the range-perpendicular compressional force that acts through mountain range forelands (Lamb, 2002; Molnar & Lyon-Caen, 1988; Monsalve et al., 2009). As a result, significant bending stress could still be supported by the lithospheric mantle. The rarity of earthquakes beneath foreland basins due to the low strain rates caused by bending in the continents ($<10^{-17}$ 1/s), particularly in the forelands of lower elevation mountain ranges that possibly have smaller in-plane compressional forces, has limited our ability to test these two competing hypotheses.

In this study, we report an unusually deep M_w 5.2 normal-faulting earthquake that occurred on the 18 November 2016 within the forelands of the southern Atlas Mountains near Biskra, Algeria (Figure 1). Our analysis of the teleseismic body-waves from this earthquake in Section 3 places the centroid at 31 km depth near the foreland Moho and, notably, 11 km deeper than any previously recognized normal-faulting earthquake beneath

21699356, 2023, 12, Downloaded from https://agupubs.onlinelibrary.wiley.com/doi/10.1029/2023JB028090 by University Of Leeds The Brotherton Library, Wiley Online Library on [10/01/2024]. See the Terms and Conditions (https://onlinelibrary.wiley.com/terms-and-conditions) on Wiley Online Library for rules of use; OA articles are governed by the applicable Creative Commons License

21699356, 2023, 12, Downloaded from https://agupubs.onlinelibrary.wiley.com/doi/10.1029/2023JB028090 by University Of Leeds The Brotherton Library, Wiley Online Library on [10/01/2024]. See the Terms and Conditions (https://onlinelibrary.wiley.com/terms-and-conditions) on Wiley Online Library for rules of use; OA articles are governed by the applicable Creative Commons License

a continental foreland basin. The depth and focal mechanism of the Biskra earthquake are unusual because they indicate that the foreland lower crust is undergoing range-perpendicular extension, which contrasts with the compressional earthquakes observed at similar depths beneath the foreland basins that wrap around the margins of Tibet and the Andes. The purpose of this study is two-fold. First, we examine what range of lithosphere rheologies can account for the observations of flexure, and the depth and mechanism of the Biskra earthquake, within the Atlas foreland. Second, we explore the possible causes of differences in the depth distribution of bending-related earthquakes between the forelands of the Atlas, Andes, and Tibet.

2. Tectonic Context

The Biskra earthquake occurred south of the range front of the Aurès Mountains, which form a part of the Atlas mountain chain of North Africa near the Algeria-Tunisia border (Figure 1a). The epicentral region is associated with an asymmetrical free-air gravity low of amplitude ∼50 mGal that has its maximum running parallel to the range front and that extends ∼200 km from the range front into the Saharan Platform (Figure 1b). The shape of the anomaly is typical of those seen globally along the margins of mountain belts caused by low-density sediments filling in a flexural depression, and can be fit by a simple model of a thin, bending plate with an effective elastic thickness T_e of at least 20 km and a plate curvature of 1–4 × 10^{-7} 1/m using the forward-modeling approach of McKenzie and Fairhead (1997) (Figure 1b).

The geological history of the region around Biskra is also consistent with the northern margin of the Saharan Platform bending due to the load of the Atlas. Surface exposure within the Aurès Mountains records a history of Mesozoic rifting during the break-up of Pangea that occurred in multiple phases between the Permian and early Cretaceous (Bracene et al., 2003). These rift sediments were then shortened as Africa drifted northwards relative to Eurasia in the Cenozoic, with the most recent major phase of shortening deforming Pleistocene sediments along the southern margin of the Aurès Mountains (Frizon de Lamotte et al., 2000). Gentle folding of Quaternary river sediments (Frizon de Lamotte et al., 2000) and GPS measurements (Bougrine et al., 2019) suggest that the range front is still active south-east of Biskra and is shortening at a rate of 1–3 mm/yr with a component of range-parallel right-lateral motion (Figure 1c). The mechanisms of shallow (i.e., <10 km) reverse and strike-slip faulting earthquakes near the range front support this view (Figure 1c). Whilst the Cenozoic rocks within the Aurès Mountains record a history of tectonic shortening, Cenozoic rocks on the Saharan Platform consist of a 1–2 km-thick sedimentary succession that has remained mostly undeformed and thickens toward the range front (Frizon de Lamotte et al., 2000; Underdown & Redfern, 2008). The geometry of these sediments, and their subsidence histories, are indicative of deposition in a foreland basin setting (Underdown & Redfern, 2008).

3. Body-Waveform Modeling of the 2016 Biskra Earthquake

The Biskra earthquake occurred at 07:42 UTC on the 18 November 2016 with a centroid determined by the global Centroid Moment Tensor (gCMT) catalog at 24 km depth (Dziewonski et al., 1981; Ekström et al., 2012) and a hypocenter in the ISC-EHB catalog at 21 km depth (Weston et al., 2018). Routine earthquake depth estimates from the gCMT and ISC-EHB may carry significant errors and uncertainties, particularly for shallow events within the crust, because of the limited sensitivity of long-period waveforms and direct-phase travel times to earthquake depths (e.g., Maggi et al., 2000). Therefore, we manually re-analyzed the teleseismic waveforms of the Biskra earthquake to determine its depth, focusing particularly on identifying surface-reflected depth phases within the *P*-wave coda.

The *P*-wave first arrivals on vertical-component seismograms at teleseismic distances (30–90°) and at all back-azimuths had dilatational arrivals, with those at the north-eastern most stations having low-amplitude first arrivals suggesting they are near nodal (Figure 2a). Potential phase arrivals were also evident within the *P*-wave coda 10–15 s after the *P*-wave arrival (Figure 2a). We first beamformed the vertical-component waveforms measured at the small-aperture seismic arrays at Kurchatov (KU: Kazaakhstan), Yellowknife (YK: Canada), and Pinedale (PD: USA) to confirm that the energy within the coda at 10–15 s derived from the same back-azimuth as the mainshock (Figure S1 in Supporting Information S1). We also performed beamforming and phase-weighted stacking of vertical-component waveforms across a medium-aperture sub-array of stations at 40.3 epicentral degrees from the source, which demonstrates that the arrivals are also coherent in slowness and have the opposite polarity to the direct arrival in this epicentral distance range (Figure 2b). The arrival times of the coda phases relative to the direct *P*-wave do not move-out significantly as a function of epicentral distance, and the phases

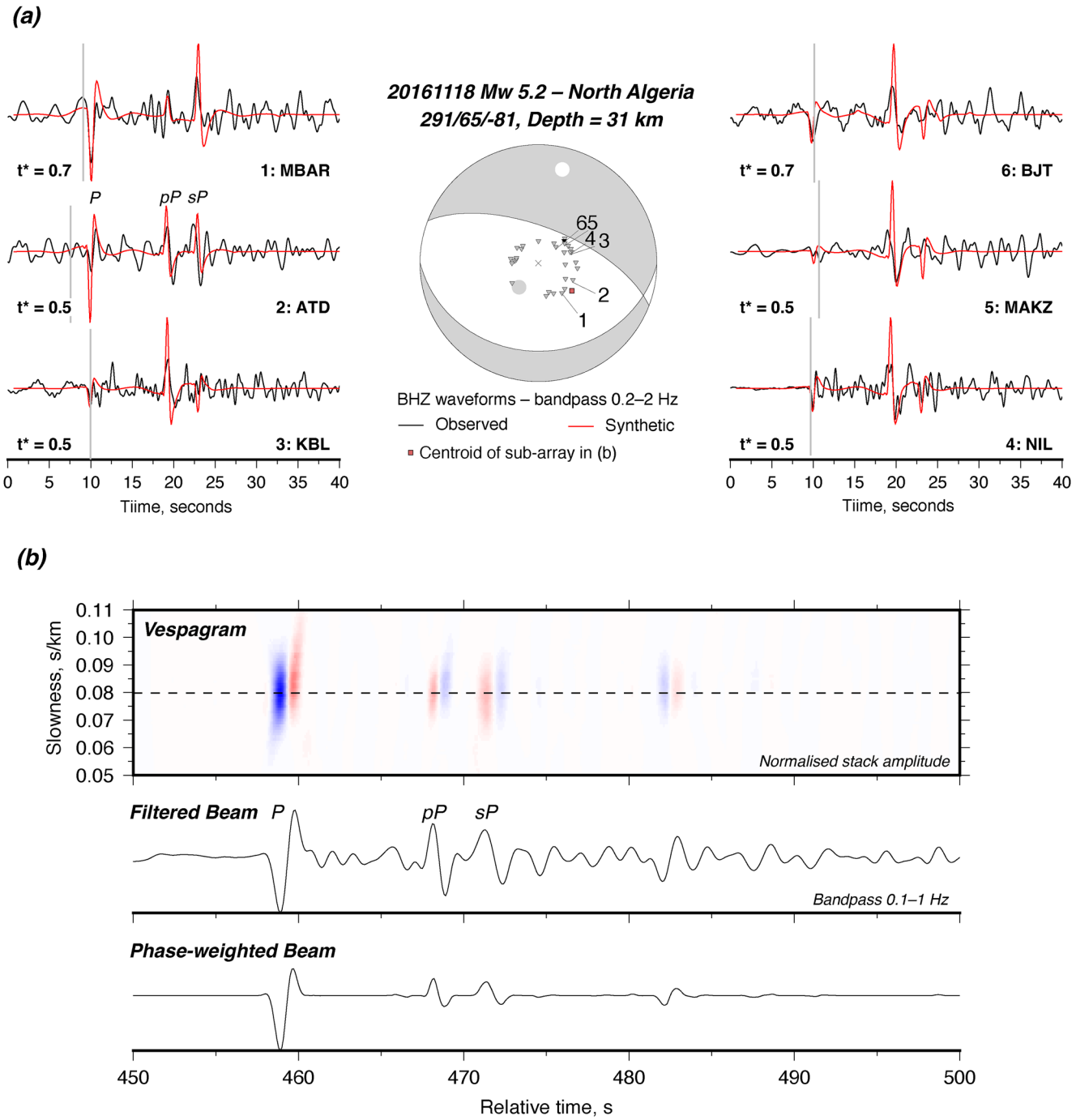

Figure 2. Teleseismic body-waveform analysis of the 18 November 2016 Biskra earthquake. (a) Forward modeling of the broadband vertical-component waveforms. The mechanism was taken from the global CMT and was updated to have a 10° steeper dip for the north-dipping nodal plane. The vertical gray lines on each waveform show the estimated arrival time of the direct *P*-phase based on the ISC hypocentral location and the IASP91 travel times. (b) Vespagram, filtered beam and phase-weighted beam for stations within a medium aperture sub-array formed of stations at 40.3 epicentral degrees demonstrating coherent arrivals 9 and 12 s after the direct arrival, which we interpret as the *pP* and *sP* depth phases. The dashed line in the vespagram shows the slowness with peak amplitude in the stack. The centroid location of the sub-array is shown on the focal sphere in (a).

appear as a pair at station ATD (Figure 2a) and in the medium-aperture array analysis (Figure 2b). We interpret these arrivals to be the principal surface-reflected depth phases *pP* and *sP*.

To determine the centroid depth of the Biskra earthquake we modeled the waveforms of the *P*, *pP* and *sP* phases assuming the earthquake source can be approximated by an instantaneous rupture at a point in space using the

21699356, 2023, 12, Downloaded from https://agupubs.onlinelibrary.wiley.com/doi/10.1029/2023JB028090 by University Of Leeds The Brotherton Library, Wiley Online Library on [10/01/2024]. See the Terms and Conditions (https://onlinelibrary.wiley.com/terms-and-conditions) on Wiley Online Library for rules of use; OA articles are governed by the applicable Creative Commons License

21699356, 2023, 12, Downloaded from https://agupubs.onlinelibrary.wiley.com/doi/10.1029/2023JB028090 by University Of Leeds The Brotherton Library, Wiley Online Library on [10/01/2024]. See the Terms and Conditions (https://onlinelibrary.wiley.com/terms-and-conditions) on Wiley Online Library for rules of use; OA articles are governed by the applicable Creative Commons License

WKBJ algorithm of Chapman (1978) and the ak135 velocity model of Kennett et al. (1995). We applied a t^* attenuation filter (Futterman, 1962) and a zero-phase bandpass filter between 0.5 and 2.0 Hz to both the synthetic and observed waveforms to remove high-frequency features related to source-time function and noise (see Maggi et al., 2000). We found that the gCMT mechanism satisfied the majority of the *P*-wave arrival polarities and relative amplitudes, but the north-dipping nodal plane needed to have a ∼10° steeper dip to account for the low amplitude *P*-wave arrivals recorded at stations north of the earthquake epicenter. For this updated mechanism the best fit between the synthetics and the observed waveforms occurred at a centroid depth of 31 km (Figure 2a), with an uncertainty related to waveform matching of ±1 km. The best-fit centroid depth is 7 km deeper than the gCMT estimate, which has only a minor effect on the predicted take-off angles and is therefore likely to have only a minor effect on the best-fit earthquake mechanism (Craig et al., 2023).

Uncertainties of ±10% in V_p and V_s above the earthquake centroid contribute a further ±2 km of uncertainty, yielding a centroid depth estimate in the range 28–34 km. The Moho depth in the region has been mapped through deep seismic soundings conducted by the European Geotraverse at ∼34–38 km in the foreland of the Tunisian Atlas (Morelli & Nicolich, 1990). Therefore, the Biskra earthquake demonstrates that the lower crust is seismogenic and in range-perpendicular extension along the northern margin of the Saharan Platform in Algeria.

3.1. Tectonic Interpretation

Active reverse faulting within and along the margins of the Atlas Mountains suggests that the stress field within the lithosphere is dominantly associated with NNW–SSE compression (Heidbach et al., 2010). Buoyancy forces acting between the Atlas Mountains and the Saharan Platform are also likely to place the foreland into range-normal compression in the absence of other forces (Molnar & Lyon-Caen, 1988). However, the normal-faulting mechanism of the Biskra earthquake is not consistent with a range-normal compressional stress state.

One potential explanation for the normal-faulting mechanism of the Biskra earthquake is that it is associated with localized transtension along the range front, but this is not supported by the GPS velocities measured either side of the earthquake epicenter (Figure 1a). We hypothesize that the horizontal stresses generated by flexure of the Saharan Platform may be large enough to adjust the stress state and place the lower crust into a state of range-normal extension. We explore this possibility below using analytical and numerical modeling of lithospheric flexure.

4. Modeling of the Stresses in the Atlas Foreland

The Biskra earthquake occurred in a section of the Saharan Platform with a free-air gravity low that runs parallel to the Atlas range front for 400 km along-strike. The earthquake also had a mechanism with both nodal planes sub-parallel to the Atlas range front (Figure 1a). Based on the shape of the gravity anomalies, we simplify our analysis of the stresses within the Saharan Platform generated by flexure to two-dimensional plane stress, and assume that strains along-strike are negligible. We also make the assumption that the strong part of the flexed lithosphere is thin relative to the wavelength of flexure (∼200 km in Figure 1a) and the bending strains are small. Under these standard assumptions the deflection of the lithosphere's surface can be approximated by the theory of a thin, bending plate overlying an inviscid half-space subject to forces and bending moments on its edge (e.g., Turcotte & Schubert, 2002). The differential stresses within the plate $\Delta\sigma_{xx} = \sigma_{xx} - \sigma_{zz}$ are related to the bending moment M and in-plane force F_x:

$$M(x) = \int_0^{z_l} z' \Delta\sigma_{xx}(x)\, dz \tag{1}$$

$$F_x = \int_0^{z_l} \Delta\sigma_{xx}(x)\, dz \tag{2}$$

where z_l is the thickness of the plate and z' is the distance from the neutral surface. Equations 1 and 2 are independent of the assumed plate rheology or boundary conditions (Turcotte & Schubert, 2002). In what follows, we use the convention that positive differential stresses ($\sigma_{xx} > \sigma_{zz}$) are associated with a stress state that promotes extensional faulting.

Faulting within the foreland lithosphere suggest that some fraction of the bending strains are accommodated through plastic (non-recoverable) deformation. We therefore model the stress-strain due to flexure as an elastic

21699356, 2023, 12, Downloaded from https://agupubs.onlinelibrary.wiley.com/doi/10.1029/2023JB028090 by University Of Leeds The Brotherton Library, Wiley Online Library on [10/01/2024]. See the Terms and Conditions (https://onlinelibrary.wiley.com/terms-and-conditions) on Wiley Online Library for rules of use; OA articles are governed by the applicable Creative Commons License

perfectly-plastic process (McAdoo et al., 1978). From the surface down to a depth H, we assume that stress in the plate can build up elastically but is limited by frictional resistance to slip on faults that increases linearly with depth (the "brittle layer") (Goetze & Evans, 1979). We express the linear increase in the limiting stress as an effective coefficient of friction on faults dipping at 45°, but the functional form could also approximate some depth-average of a more complex stress-depth limit that includes processes like semi-brittle deformation. We interpret the Biskra earthquake to indicate that the plate can remain brittle and seismogenic to at least 31 ± 3 km depth.

Beneath the brittle layer, as temperature in the lithosphere increases with depth, crystal-plastic deformation mechanisms including low-temperature plasticity and dislocation creep will limit the size of the elastic stresses (Goetze & Evans, 1979). These creep mechanisms are strain-rate dependent, meaning that the limit on the elastic stresses will depend on the rate at which the plate is being bent. The axial strain rates associated with flexure in Algeria will be small (10^{-19}–10^{-21} 1/s) compared to typical rates of deformation in active settings (10^{-14}–10^{-15} 1/s) due to the small plate curvatures (1–4 × 10^{-7} 1/m) and underthrusting rates (1–3 mm/yr). Figure S2 in Supporting Information S1 shows predictions of the stress needed to deform a lithospheric mantle formed of dry olivine at the strain rates caused by bending. For reasonable differential stresses (<500 MPa) and at depths >30 km the stresses in the mantle are expected to be limited by dislocation creep and can be approximated by a function of the form $\sigma_0 \exp(-z/z_r)$ where $z_r \approx 5$ km (Lavier & Steckler, 1997). Therefore, we make the simplification that the limit on the elastic stresses below the brittle layer follows an exponential decay down to the base of the plate, and present results of modeling with different assumed z_r. Using this simplified functional form, we implicitly model the effects of different bending strain rates on the plate rheology by allowing the brittle layer thickness to vary, with thicker brittle layers reflecting higher strain-rate conditions.

The rheological model described above replicates the single-layer model for cratonic lithosphere (Jackson, 2002; Watts & Burov, 2003). We do not consider a multi-layer rheology with widespread ductile yielding in a weak lower crust bracketed by a strong, brittle layer above and below (Burov & Diament, 1995) because the Biskra earthquake suggests that the elastic stresses that can build up in the lower crust are limited by resistance to seismogenic slip on faults.

We have also not included any visco-elastic effects (e.g., Kusznir, 1991; Ellis & Wang, 2022) and assume that the deflection of the lithosphere can be modeled by static loading. Visco-elasticity has the effect of introducing time-dependence to the stress distribution following the application of a load, such that stresses associated with past episodes of loading can remain "frozen in" to the lithosphere. Ellis and Wang (2022) showed that the time-scale for the change in stress state within the cold, elastic portion of cratonic lithosphere following a change in horizontal loading is on the order of ~5–10 Myrs. Given that the Atlas and its forelands have been undergoing shortening and loading in the current tectonic configuration throughout the Cenozoic, and given that we are not trying to derive the values of the loads but rather the stresses within the plate, then we believe it is reasonable to model the loads using a static approximation (see also Monsalve et al., 2009).

4.1. Analytical Modeling

The depth of normal-faulting earthquakes within the foreland lithosphere places a bound on the depth to which the stresses generated by flexure are equivalent to the stresses needed to break normal faults ('extensional yielding'). To gain insight into the controls on the depth of extensional yielding, we constructed a semi-analytical model using Equations 1 and 2, plus the condition that the plate curvature is related to the stress gradient within the plate's elastic core (e.g., Lavier & Steckler, 1997):

$$\frac{d^2w}{dx^2} = \frac{\left(1-\upsilon^2\right)}{E}\frac{d\Delta\sigma_{xx}}{dz}, \tag{3}$$

where w is the deflection, $E = 70$ GPa is Young's modulus, and $\upsilon = 0.25$ is Poisson's ratio. From Equations 1–3, if the curvature of the lithosphere and the in-plane force F_x can be estimated, then we can determine the relationships between the depth of extensional yielding and the parameters that control the lithosphere's rheology (H, μ', z_r) in our simplified model set-up. The resulting solutions are semi-analytical, as we solve Equations 1 and 2 using numerical integration.

For the modest plate curvatures in the Saharan Platform on the southern margin of the Atlas mountains (~3 × 10^{-7} 1/m), the depth of extensional yielding is mostly dependent on the brittle-layer thickness H and less so on the

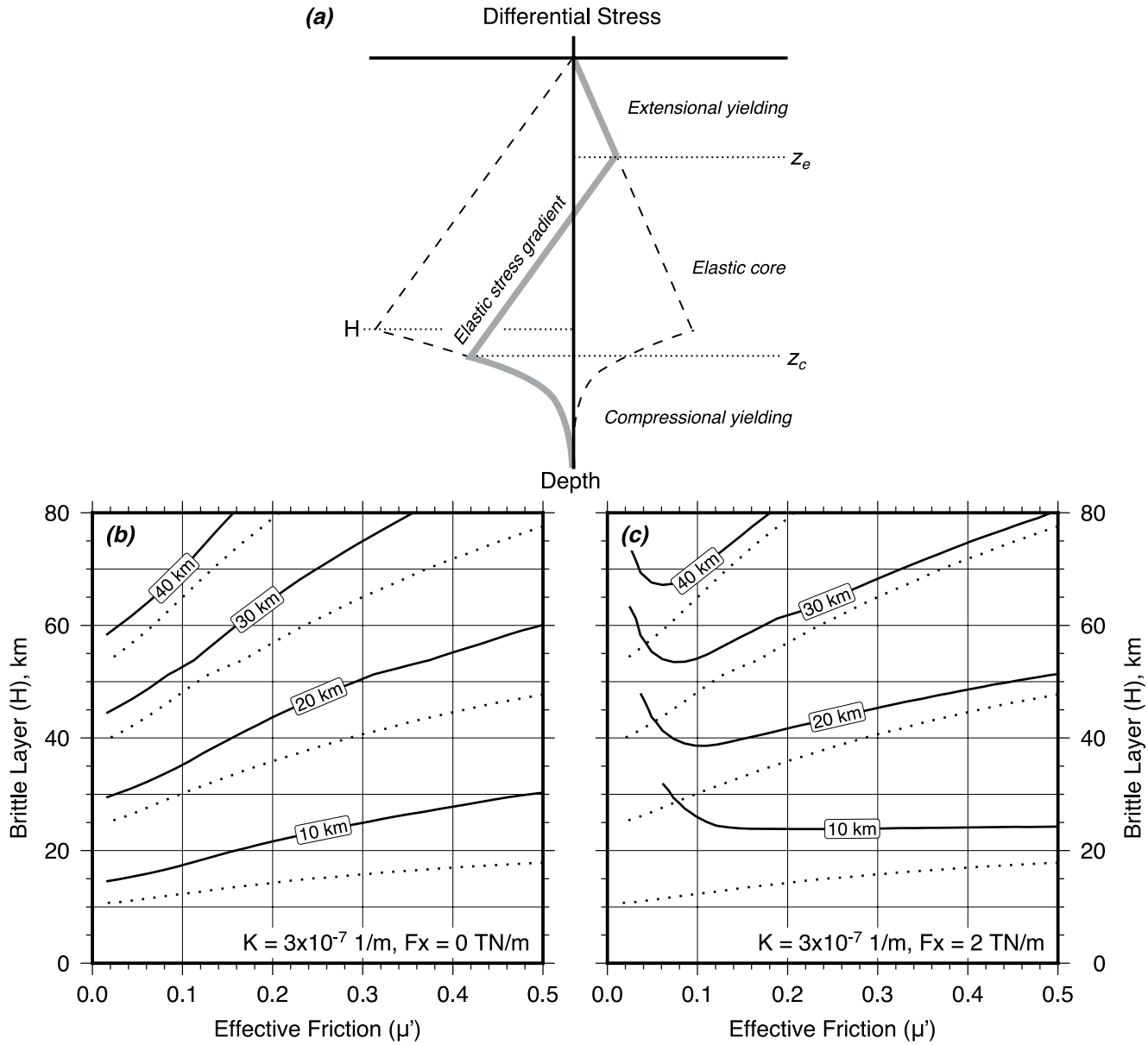

Figure 3. Semi-analytical solutions for the depth of extensional yielding within an elastic-plastic plate of curvature 3×10^{-7} 1/m. (a) Sketch of the stress distribution (thick gray line) and maximum stresses (black dashed line) supportable by the lithosphere with depth. (b) Depth of extensional yielding z_e assuming no in-plane force and a $z_r = 0$ km (solid line) or $z_r = 5$ km (dotted line). (c) Depth of extensional yielding when adding an in-plane force of $F_x = 2$ TN/m (solid line) compared to $F_x = 0$ TN/m (dotted line). All calculations in (c) assume $z_r = 5$ km.

effective frictional strength of faults within the brittle layer μ' (Figure 3a). For brittle layers similar in thickness to typical foreland crust (~30–40 km), extensional yielding can occur down to ~10–25 km depth for $\mu' = 0.1$–0.6. Increasing the stresses supported in the lithospheric mantle by increasing z_r or increasing H has the effect of increasing the depth of extensional yielding for a fixed F_x (Figure 3a), because of the need to balance the larger contribution of bending stresses to the bending moment below the neutral surface (Equation 1). For the equivalent H-μ' range, but with an in-plane compression of 2 TN/m that simulates a small buoyancy force acting between the mountains and forelands, the neutral surface is shifted shallower and the depth of extensional yielding decreases to 10–15 km (Figure 3b). A tensional in-plane force would increase the depth of extensional yielding, but this scenario is unlikely in a foreland setting.

These simple calculations demonstrate that, if the Saharan Platform is in net compression, then for the estimated plate curvature no models have a depth of extensional yielding of ~30 km in a brittle layer H that is similar

21699356, 2023, 12, Downloaded from https://agupubs.onlinelibrary.wiley.com/doi/10.1029/2023JB028090 by University Of Leeds The Brotherton Library, Wiley Online Library on [10/01/2024]. See the Terms and Conditions (https://onlinelibrary.wiley.com/terms-and-conditions) on Wiley Online Library for rules of use; OA articles are governed by the applicable Creative Commons License

Table 1
Parameter Range Searched in the Numerical Models Described in Section 4.2

Parameter	Minimum	Maximum
H	5 km	100 km
μ'	0.01	0.6
F_z	10^{10} TN/m	10^{14} TN/m
F_x	10^{10} TN/m	10^{14} TN/m
M	10^{15} N	10^{19} N
x_0	−300 km	0 km
$\Delta\rho$	600 kg/m^3	900 kg/m^3

Note. The parameter notation is explained in the text. The range of density contrast between the sediment and the mantle $\Delta\rho$ is based on the petrophysical properties of the Ghadames Basin in Underdown and Redfern (2008).

in thickness to the crust (34–38 km; Morelli and Nicolich (1990)). In addition, the lower bending strain rates expected within the Saharan Platform compared with those in the Indian or Brazilian Shields should lead to shallower extensional yielding in Algeria, not deeper like observed. The lithospheric mantle may therefore need to support a fraction of the differential stresses generated by flexure in the Atlas foreland to account for the depth of the Biskra earthquake.

4.2. Numerical Modeling

In practice the stress distribution within the lithosphere will vary as a function of distance from the range front in tandem with variations in the plate curvature. In this section, we employ a simple two-dimensional numerical model of plate bending in response to static loading to determine the range of lithosphere rheologies that can account for both the shape of the free-air gravity anomalies, which reflect the plate curvature, and the depth of normal faulting in the Saharan Platform.

We model the bending of a thin plate subject to arbitrary end-loads and moments following Burov and Diament (1992), and solve the relevant equations of plate flexure using the open-source finite-difference code tAo (Garcia-Castellanos et al., 1997). On the foreland boundary of the model x_{max}, we apply the condition that $w(x = x_{max}) = 0$. Along the boundary of the plate beneath the mountains x_0, we apply the condition that the vertical shear force V on the plate end is $V(x = x_0) = 0$, which is equivalent to assuming the plate is broken. The range front is positioned at $x = 0$. We also tested models with a continuous plate boundary condition (i.e., $w'(x = x_0) = 0$), though found it did not change the model results as the best-fit position of x_0 was typically far from the range front ($x_0 \ll 0$). We computed gravity anomalies from the modeled deflection using the plate approximation $\Delta g(x) = 2\pi G\Delta\rho w(x)$, where G is the gravitational constant and $\Delta\rho$ is the density contrast between basin sediment and mantle (see a sketch of the model set-up in Figure S3 in Supporting Information S1).

To determine the range of models that match the gravity and earthquake observations, we performed a Monte Carlo search of the parameter space with a non-linear least-squares minimization step to solve for nuisance parameters. The free parameters were the vertical force acting on the edge of the plate $F_z(x = x_0)$, the in-plane force F_x, bending moment $M(x = x_0)$, the location of the plate break x_0, the density contrast between basin sediment and mantle $\Delta\rho$, and the brittle layer thickness H and effective static friction of faults μ' (see Table 1 for parameter ranges). We assumed that the foreland is in horizontal net compression due to the buoyancy forces acting between the Atlas Mountains and Saharan Platform. The nuisance parameters consist of a static offset and linear ramp added to the modeled gravity data to account for long-wavelength contributions to the gravity field from mantle flow. We searched over 1 million different combinations of parameters, and stored the models that match the gravity data with $\chi^2 \leq 1.5\chi^2_{min}$ and which experienced plastic yielding in horizontal extension at > 28 km depth south of the range front. Increasing the number of parameter combinations did not change the range of models that matched the data, suggesting the inferences we draw from this sample are robust.

We find that plate models can match the gravity data to within the uncertainty bound as long as $H \geq 20$ km (Figure 4a). The largest misfits between the models and observations occur within 20–40 km of the range front where the gravity anomaly has an inflexion to become concave up, which most likely represents aliasing of the positive free-air gravity high in the mountains with the free-air gravity low in the foreland basin. By including the constraint that the models need to match both the gravity data and the depth of extensional yielding inferred from the Biskra earthquake, the brittle layer H needs to be > 40 km thick and contain faults with $\mu' > 0.025$ (Figures 4b and 4c). The models constrain the lower bound on the brittle layer thickness for two reasons. Firstly, by selecting models with extensional yielding down to >28 km depth we implicitly assume the brittle layer must be at least this thick. Secondly, the lithosphere needs to be strong enough to match the shape of the gravity anomalies. Lithosphere with a brittle layer less than 40 km thick, and which is yielding at > 28 km depth, produces a short-wavelength deflection that is not consistent with the shape of the observed free-air gravity anomaly. The lower bounds the numerical models place on H and μ' are similar to those inferred from the semi-analytical models in Section 4.1, and require that at least the top 5–10 km of the lithospheric mantle beneath the Saharan Platform supports bending-related stresses through elastic resistance to deformation. A compilation of the stress

21699356, 2023, 12, Downloaded from https://agupubs.onlinelibrary.wiley.com/doi/10.1029/2023JB028090 by University Of Leeds The Brotherton Library, Wiley Online Library on [10/01/2024]. See the Terms and Conditions (https://onlinelibrary.wiley.com/terms-and-conditions) on Wiley Online Library for rules of use; OA articles are governed by the applicable Creative Commons License

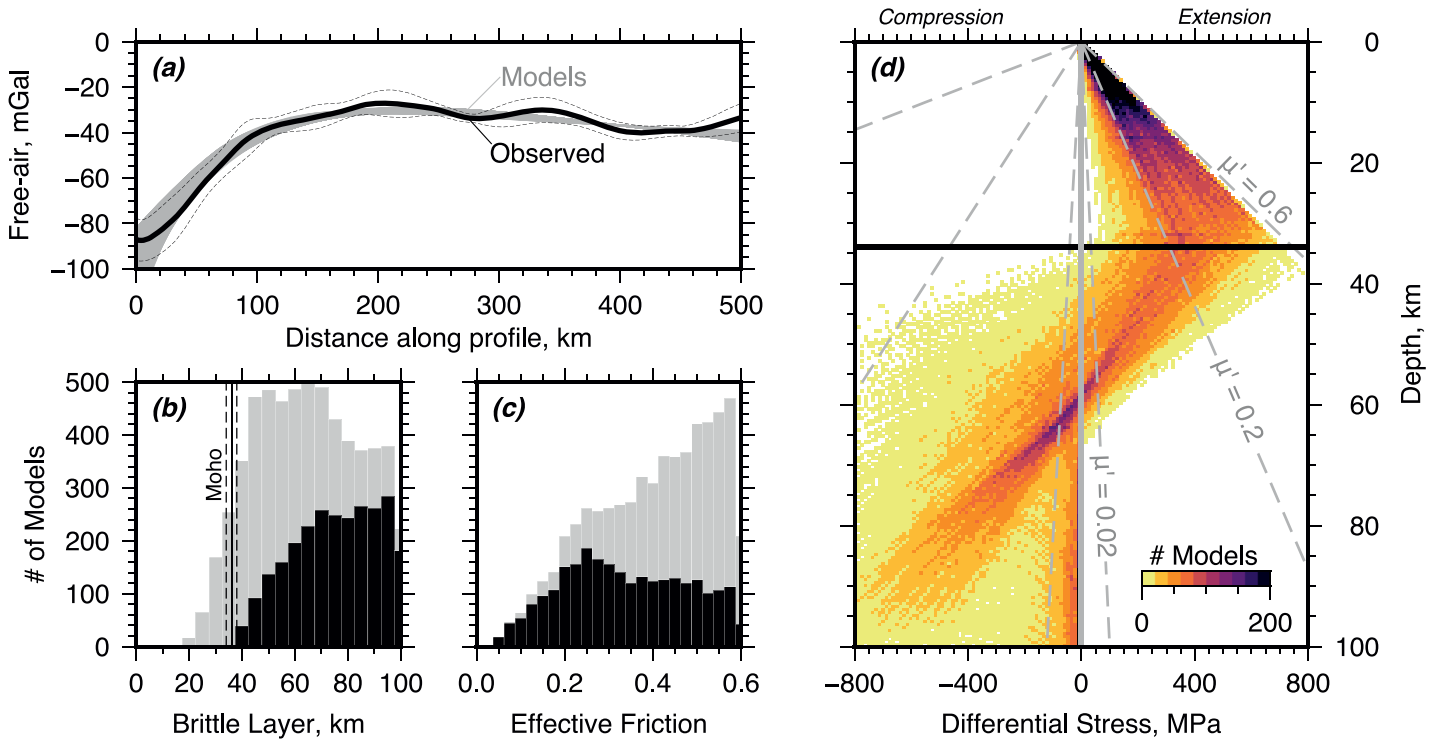

Figure 4. Results of the Monte-Carlo search for models that match the observed free-air gravity observations and the depth of extensional faulting in the Biskra earthquake. (a) Observed and modeled free-air gravity profiles for models with a $\chi^2 \leq 1.5\ \chi^2_{min}$. (b) and (c) are histograms of the brittle layer thickness (h) and effective friction (μ') for models that either fit just the gravity (gray bars), or fit both the gravity and earthquake observations (black bars). The Moho depth is taken from the seismic section of Morelli and Nicolich (1990). (d) Differential stress within the plate taken from the location foreland-ward of the range front where the depth of extensional yielding is at a maximum. Predictions for the differential stresses needed to break faults with various μ' that dip at 45° using an average lithosphere density of 2,800 kg/m^3 are shown as gray dashed lines.

distributions at the point within the foreland where the depth of extensional yielding is at its maximum shows that, immediately below the Moho, these elastic stresses are at least ~40 MPa (Figure 4d).

Increasing the brittle layer thickness beyond 40 km has little effect on the model fits, because thicker brittle layers are able to match the gravity data and depth of extensional yielding by increasing the forces deforming the lithosphere, reducing the effective friction, by having larger distances to the load point x_0, or by a combination of these three factors (Figure S4 in Supporting Information S1). These various trade-offs mean that, similar to the forward modeling approaches for estimating the effective elastic thickness from gravity profiles (e.g., McKenzie & Fairhead, 1997), we cannot constrain the upper bound on the brittle layer thickness. Similarly, we cannot place an upper bound on the amplitude of the differential stresses within the crust or lithospheric mantle caused by bending.

5. Discussion

Our modeling of the stress distribution within the Atlas foreland places useful new constraints on the rheology of the continental lithosphere in northern Africa, and on the geodynamics of flexural foreland regions worldwide. In order to account for the depth of extensional faulting near Biskra, we find that the lithospheric mantle of the Saharan Platform needs to support bending stresses on the order of a few 10s of MPa elastically down to depths at least 5–10 km below the Moho. In addition, the Biskra earthquake demonstrates that the lower crust beneath the Saharan Platform is seismogenic, and therefore needs to be able to sustain enough elastic stress to rupture faults.

The constraints on the rheology of the Saharan Platform are similar to those determined for the Indian lithosphere where it underthrusts the southern margin of Tibet. Within the Indian lithosphere, earthquakes have been found to occur throughout the crust (Bodin & Horton, 2004) and are now believed to extend up to ~10 km below the Indian Moho beneath the Himalaya (Craig et al., 2012; Schulte-Pelkum et al., 2019), indicating that the lower crust and upper mantle is able to accumulate and release elastic strain in earthquakes at stresses lower than those needed to deform by crystal-plastic creep (Monsalve et al., 2009). The Indian lithosphere is thought to be strong enough

21699356, 2023, 12, Downloaded from https://agupubs.onlinelibrary.wiley.com/doi/10.1029/2023JB028090 by University Of Leeds The Brotherton Library, Wiley Online Library on [10/01/2024]. See the Terms and Conditions (https://onlinelibrary.wiley.com/terms-and-conditions) on Wiley Online Library for rules of use; OA articles are governed by the applicable Creative Commons License

Table 2
Summary of the Plate Curvature K, In-Plane Force F_x, Depth of Extensional Faulting z_e, Depth of Compressional Faulting z_c, and Sediment Thickness z_s Within the Forelands of Mountain Ranges With Shallow Normal Faulting

Foreland	K, 10^{-7} 1/m	F_x, TN/m	z_e, km	z_c, km	z_s, km
Algeria	1.4–4.5	1.0	31	–	3
Colombia	0.9–2.5	3.5	18	28(?)	4
South Peru	0.9–2.6	4.5	7	31	5
India	0.6–1.4	5.0	20	51	7

Note. The range in curvature accounts for density contrasts between sediment and mantle $\Delta\rho$ of between 600 kg/m^3 and 900 kg/m^3 and were estimated using the flexural profiles in Figure 1 and Figures S6–S8 in Supporting Information S1. Earthquake centroid depths are all derived from body-waveform modeling and are taken from the gWFM catalog (Wimpenny & Watson, 2020). The depth of compressional seismicity in the Colombian foreland is uncertain, as the epicentral uncertainty on the location of the compressional earthquake means it could be associated with a range front thrust and not be within the underthrusting Brazilian Shield. Sediment thicknesses are taken from Laske and Masters (1997).

to accumulate elastic stresses into the upper mantle through the combination of a relatively thin, anhydrous crust, and a cold uppermost mantle, thermally (and possibly chemically) insulated from the hot convecting mantle by a ∼200 km-thick lithospheric keel (Priestley et al., 2008). Recently published multi-mode surface-wave tomography shows that the similarly thick lithosphere previously known to underlie the West African Craton also extends beneath the southern Atlas foreland and is 150–180 km-thick beneath Biskra (Priestley & McKenzie, 2013; Celli et al., 2020). We constructed geotherms using the lithosphere and crustal thickness estimates near Biskra using the method of McKenzie et al. (2005) and, for the expected axial strain rates associated with bending (10^{-19}–10^{-21} 1/s), laboratory-derived flow laws for dry olivine (Hirth & Kohlstedt, 2003; Mei et al., 2010) predict that the top 10 km of the lithospheric mantle of the Saharan Platform could well be cool enough to support differential stresses of a few 10s of MPa elastically (Figure S5 in Supporting Information S1). However, the range of models in which elastic stresses of 100's of MPa are supported within the upper mantle appear unlikely even if it is formed of dry olivine, as the required bending strains could be accommodated at differential stresses $\ll$100 MPa by dislocation creep. Importantly, these results indicate that the lithospheric mantle does support a significant fraction of the bending stresses in the Algerian foreland lithosphere, even though the strain rates associated with bending are at least one order of magnitude less than those in the Indian lithosphere as it underthrusts Tibet.

If the lithosphere surrounding the margins of Tibet and the Andes has a similar rheology to the Saharan Platform, this raises the question: why is the depth of extensional faulting so much deeper in the Atlas foreland? One of the key differences between the Tibetan, Andean and Atlas forelands is the amplitude of the buoyancy force that places the foreland lithosphere into net compression (Molnar & Lyon-Caen, 1988). These buoyancy forces derive predominantly from contrasts in crustal thickness between the mountain range and its forelands, and are related to the relief h of the mountain range above its forelands (Molnar & Lyon-Caen, 1988). Estimates of the buoyancy force acting through the Indian lithosphere are on the order of 5–6 TN/m (h = 5,000 m) (Copley et al., 2010), within the Brazilian Shield near the central Andes they are 4–6 TN/m (h = 4,500 m) (Lamb, 2000), and within the northern Andes they are 3–4 TN/m (h = 3,000 m) (Wimpenny, 2022). A similar calculation for the Atlas Mountains, which has an average relief of h = 1,500 m, results in a buoyancy force of 1–2 TN/m. If larger buoyancy forces equate to a larger in-plane compression acting through the adjacent forelands, then forelands of high mountains may be expected to have a shallower neutral surface and shallower normal faulting seismicity. We performed a simple test of this hypothesis using the semi-analytical modeling approach described in Section 4.1.

We selected the four continental foreland basins that have well-recorded normal-faulting seismicity (see Table 2), and calculated the range of plausible plate curvatures from the free-air gravity anomalies (Figures S6–S8 in Supporting Information S1). We then assumed that the buoyancy forces acting between the mountains and lowlands are equivalent to the in-plane force F_x, and computed the depth of extensional and compressional yielding as a function of the brittle layer thickness H and effective friction of faults μ' in the brittle layer. Figure 5a shows the range of H-μ' that is consistent with the observed depth-extent of normal and reverse faulting in each foreland. The depth distribution of seismicity in all four settings can be explained if the lithosphere has $\mu' \approx 0.025$–0.1 and $H \gtrsim 50$ km (Figure 5a). The small size of the region of overlap in Figure 5a is somewhat artificial, as it is sensitive to the assumptions about the uncertainties in the depth of earthquakes and the shape of the yield strength envelope in the lithospheric mantle. Nevertheless, these simple calculations demonstrate that if the upper ∼10–20 km of the lithospheric mantle is able to support bending stresses, then a smaller in-plane compression in the forelands of the Atlas compared to that in the forelands of Tibet and the Andes provides a simple explanation for the differences in the depth of extensional faulting between these settings (Figure 5b).

21699356, 2023, 12, Downloaded from https://agupubs.onlinelibrary.wiley.com/doi/10.1029/2023JB028090 by University Of Leeds The Brotherton Library, Wiley Online Library on [10/01/2024]. See the Terms and Conditions (https://onlinelibrary.wiley.com/terms-and-conditions) on Wiley Online Library for rules of use; OA articles are governed by the applicable Creative Commons License

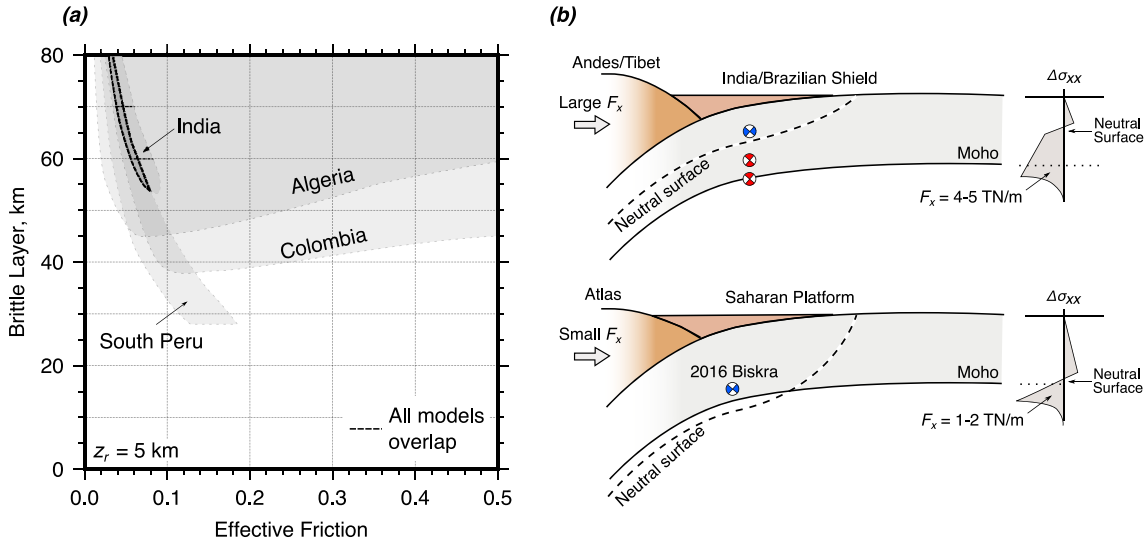

Figure 5. Summary of the differences in the depth distribution of seismicity between the Atlas, Tibetan and Andean forelands and its links with lithosphere rheology. (a) Calculations showing the range of effective friction μ' and brittle layer thickness H values that can account for the depth distribution of earthquakes, plate curvature and in-plane force in four different foreland settings. Details of the parameters used in each calculation are shown in Table 2. Each foreland is represented as a gray polygon, with darker areas showing areas where the same H-μ' combination can account for the observations from multiple foreland settings. The dashed black line shows the location in H-μ' space where a single lithosphere rheology can explain the faulting, curvature and in-plane force observations from all four settings considered here. (b) Sketch interpretation for the differences in the depth of seismicity between the forelands of the Andes, Atlas, and Tibet.

6. Conclusions

The 2016 Biskra normal-faulting earthquake was unusual in that it ruptured the lower crust of the foreland lithosphere bounding the Algerian Atlas Mountains. We have shown that simple models of lithospheric flexure can account for the depth and mechanism of the Biskra earthquake and gravity anomalies within the region, but indicate that at least the top 5–10 km of the foreland lithospheric mantle support bending stresses of a few 10s of MPa elastically. The southern margin of the Atlas is underlain by moderately thick lithosphere, which may lead to a cool and thereby strong upper mantle that can support these bending stresses, even at the low axial strain rates associated with the underthrusting of the Saharan Platform beneath the Atlas Mountains (10^{-19}–10^{-21} 1/s). Differences in the depth distribution and mechanisms of earthquakes between the forelands of the Andes, Tibet and the Atlas can be explained if these foreland regions have similar rheologies but have different in-plane compressional forces that are roughly equivalent to the buoyancy forces acting between the mountains and their lowlands. Our findings indicate that the strong continental lithosphere bounding mountain ranges supports significant differential stresses within at least the top 5–10 km of the upper mantle.

Data Availability Statement

All data used in this study are openly available. All seismic data were downloaded through the EarthScope Consortium Wilber 3 system (https://ds.iris.edu/wilber3/) and derive from the Global Seismographic Network (GSN) (https://doi.org/10.7914/SN/IU) (Albuquerque Seismological Laboratory (ASL)/U.S. Geological Survey (USGS), 2014) and the Geoscope network (https://doi.10.18715/GEOSCOPE.G) (Institut de physique du globe de Paris (IPGP) and Ecole et Observatoire des Sciences de la Terre de Strasbourg (EOST), 1982). The GSN is a cooperative scientific facility operated jointly by the National Science Foundation (NSF) and the United States Geological Survey (USGS) The NSF component is part of NSF's SAGE Facility, operated by EarthScope Consortium under Cooperative Support Agreement EAR-1851048. The computer program tAo used for modelling lithospheric flexure is available from https://sites.google.com/site/daniggcc/software/tao (last accessed May 2023). All of the codes and raw data files needed to reproduce the data processing and modelling results are available from https://doi.org/10.5281/zenodo.10262403 (Wimpenny, 2023). Obspy was used in the seismic data processing (Beyreuther et al., 2010).

21699356, 2023, 12, Downloaded from https://agupubs.onlinelibrary.wiley.com/doi/10.1029/2023JB028090 by University Of Leeds The Brotherton Library, Wiley Online Library on [10/01/2024]. See the Terms and Conditions (https://onlinelibrary.wiley.com/terms-and-conditions) on Wiley Online Library for rules of use; OA articles are governed by the applicable Creative Commons License

Acknowledgments
SW and TC were supported in this work by the Royal Society under URF\R1\180088 and RF\ERE\210041, and also through COMET, which is the NERC Centre for the Observation and Modelling of Earthquakes, Volcanoes and Tectonics, a partnership between UK Universities and the British Geological Survey. AB was supported by the Leeds-York-Hull Natural Environment Research Council (NERC) Doctoral Training Partnership (DTP) Panorama under grant NE/S007458/1. The numerical modelling component of this work was undertaken on ARC4, part of the High Performance Computing facilities at the University of Leeds, UK. We thank the Editor, Rachel Abercrombie, one anonymous reviewer and Simon Lamb for their constructive reviews.

References

Albuquerque Seismological Laboratory (ASL)/U.S. Geological Survey (USGS). (2014). *Global seismograph network—IRIS/USGS*. International Federation of Digital Seismograph Networks.

Baranowski, J., Armbruster, J., Seeber, L., & Molnar, P. (1984). Focal depths and fault-plane solutions of earthquakes and active tectonics of the Himalaya. *Journal of Geophysical Research*, *89*(B8), 6918–6928. https://doi.org/10.1029/jb089ib08p06918

Beyreuther, M., Barsch, R., Krischer, L., Megies, T., Behr, Y., & Wassermann, J. (2010). ObsPy: A python toolbox for seismology. *Seismological Research Letters*, *81*(3), 530–533. https://doi.org/10.1785/gssrl.81.3.530

Bodin, P., & Horton, S. (2004). Source parameters and tectonic Implications of Aftershocks of the Mw 7.6 Bhuj earthquake of 26 January 2001. *Bulletin of the Seismological Society of America*, *94*(3), 818–827. https://doi.org/10.1785/0120030176

Bougrine, A., Yelles-Chaouche, A. K., & Calais, E. (2019). Active deformation in Algeria from continuous GPS measurements. *Geophysical Journal International*, *217*(1), 572–588. https://doi.org/10.1093/gji/ggz035

Bracene, R., Patriat, M., Ellouz, N., & Gaulier, J. M. (2003). Subsidence history in basins northern Algeria. *Sedimentary Geology*, *156*(1–4), 213–239. https://doi.org/10.1016/s0037-0738(02)00289-0

Burov, E. B., & Diament, M. (1992). Flexure of the continental lithosphere with multilayered rheology. *Geophysical Journal International*, *109*(2), 449–468. https://doi.org/10.1111/j.1365-246x.1992.tb00107.x

Burov, E. B., & Diament, M. (1995). The effective elastic thickness (Te) of continental lithosphere: What does it really mean? *Journal of Geophysical Research*, *100*(B3), 3905–3927. https://doi.org/10.1029/94jb02770

Celli, N. L., Lebedev, S., Schaeffer, A. J., Ravenna, M., & Gaina, C. (2020). The upper mantle beneath the South Atlantic Ocean, South America and Africa from waveform tomography with massive data sets. *Geophysical Journal International*, *221*(1), 178–204. https://doi.org/10.1093/gji/ggz574

Chapman, C. H. (1978). A new method for computing synthetic seismograms. *Geophysical Journal International*, *54*(3), 481–518. https://doi.org/10.1111/j.1365-246x.1978.tb05491.x

Chapple, W. M., & Forsyth, D. W. (1979). Earthquakes and bending of plates at Trenches. *Journal of Geophysical Research*, *84*(B12), 6729–6749. https://doi.org/10.1029/jb084ib12p06729

Copley, A., Avouac, J. P., & Royer, J. Y. (2010). India-Asia collision and the Cenozoic slowdown of the Indian plate: Implications for the forces driving plate motions. *Journal of Geophysical Research*, *115*(3), 1–14. https://doi.org/10.1029/2009jb006634

Craig, T. J., Copley, A., & Jackson, J. A. (2012). Thermal and tectonic consequences of India underthrusting Tibet. *Earth and Planetary Science Letters*, *353–354*, 231–239. https://doi.org/10.1016/j.epsl.2012.07.010

Craig, T. J., Copley, A., & Middleton, T. A. (2014). Constraining fault friction in oceanic lithosphere using the dip angles of newly-formed faults at outer rises. *Earth and Planetary Science Letters*, *392*, 94–99. https://doi.org/10.1016/j.epsl.2014.02.024

Craig, T. J., Jackson, J., Priestley, K., & Ekström, G. (2023). A Cautionary Tale: Examples of the mis-location of small earthquakes beneath the Tibetan plateau by routine approaches. *Geophysical Journal International*, *233*(3), 2021–2038. https://doi.org/10.1093/gji/ggad025

Devlin, S., Isacks, B. L., Pritchard, M. E., Barnhart, W. D., & Lohman, R. B. (2012). Depths and focal mechanisms of crustal earthquakes in the central Andes determined from teleseismic waveform analysis and InSAR. *Tectonics*, *31*(2), 1–33. https://doi.org/10.1029/2011tc002914

Dziewonski, A. M., Chou, T.-A., & Woodhouse, J. H. (1981). Determination of earthquake source parameters from waveform data for studies of global and regional seismicity. *Journal of Geophysical Research*, *86*(B4), 2825–2852. https://doi.org/10.1029/jb086ib04p02825

Ekström, G., Nettles, M., & Dziewoński, A. (2012). The global CMT project 2004–2010: Centroid-moment tensors for 13,017 earthquakes. *Physics of the Earth and Planetary Interiors*, *200*, 1–9. https://doi.org/10.1016/j.pepi.2012.04.002

Ellis, S., & Wang, K. (2022). Lithospheric strength and stress revisited: Pruning the Christmas tree. *Earth and Planetary Science Letters*, *595*, 117771. https://doi.org/10.1016/j.epsl.2022.117771

Frizon de Lamotte, D., Saint Bezar, B., Bracene, R., & Mercier, E. (2000). The two main stepsof the Atlas building and geodynamics of the western Mediterranean. *Tectonics*, *19*(4), 740–761. https://doi.org/10.1029/2000tc900003

Futterman, W. I. (1962). Dispersive body waves. *Journal of Geophysical Research*, *67*(13), 5279–5291. https://doi.org/10.1029/jz067i013p05279

Garcia-Castellanos, D., Fernàndez, M., & Torne, M. (1997). Numerical modeling of foreland basin formation: A program relating thrusting, flexure, sediment geometry and lithospehre rheology. *Computers & Geosciences*, *23*(9), 993–1003. https://doi.org/10.1016/s0098-3004(97)00057-5

Goetze, C., & Evans, B. (1979). Stress and temperature in the bending lithosphere as constrained by experimental rock mechanics. *Geophysical Journal of the Royal Astronomical Society*, *59*(3), 463–478. https://doi.org/10.1111/j.1365-246x.1979.tb02567.x

Heidbach, O., Tingay, M., Barth, A., Reinecker, J., Kurfeß, D., & Müller, B. (2010). Global crustal stress pattern based on the World Stress Map database release 2008. *Tectonophysics*, *482*(1–4), 3–15. https://doi.org/10.1016/j.tecto.2009.07.023

Hirth, G., & Kohlstedt, D. L. (2003). Rheology of the upper mantle and the mantle Wedge: A view from the Experimentalists. *Geophysical Monograph Series*, *138*, 83–105. https://doi.org/10.1029/138gm06

Institut de physique du globe de Paris (IPGP) and Ecole et Observatoire des Sciences de la Terre de Strasbourg (EOST). (1982). *GEOSCOPE, French global network of broad band seismic stations*. Institut de physique du globe de Paris (IPGP), Université de Paris.

Jackson, J. A. (2002). Strength of the continental lithosphere: Time to abandon the jelly sandwich? *Geological Society of America Today*, *12*(9), 4. https://doi.org/10.1130/1052-5173(2002)012<0004:sotclt>2.0.co;2

Jackson, J. A., McKenzie, D., Priestley, K., & Emmerson, B. (2008). New views on the structure and rheology of the lithosphere. *Journal of the Geological Society*, *165*(2), 453–465. https://doi.org/10.1144/0016-76492007-109

Kennett, B. L. N., Engdahl, E. R., & Buland, R. (1995). Constraints on seismic velocities in the Earth from traveltimes. *Geophysical Journal International*, *122*(1), 108–124. https://doi.org/10.1111/j.1365-246x.1995.tb03540.x

Kusznir, N. J. (1991). Time distribution of stress with depth in the lithosphere: Thermo-rheological and geodynamic constraints. *Philosophical Transactions - Royal Society of London, A*, *337*(1645), 95–110.

Lamb, S. (2002). Is it all in the crust? *Nature*, *420*(6912), 130–131. https://doi.org/10.1038/420130a

Lamb, S. H. (2000). Active deformation in the Bolivian Andes, South America. *Journal of Geophysical Research*, *105*(B11), 25627–25653. https://doi.org/10.1029/2000jb900187

Laske, G., & Masters, G. (1997). A global digital map of sediment thickness. *Eos, Transactions American Geophysical Union*, *78*.

Lavier, L. L., & Steckler, M. (1997). The effect of sedimentary cover on the flexural strength of continental lithosphere. *Nature*, *389*(6650), 476–479. https://doi.org/10.1038/39004

Maggi, A., Jackson, J. A., McKenzie, D., & Priestley, K. (2000). Earthquake focal depths, effective elastic thickness, and the strength of the continental lithosphere. *Geology*, *28*(6), 495. https://doi.org/10.1130/0091-7613(2000)28<495:efdeet>2.0.co;2

21699356, 2023, 12, Downloaded from https://agupubs.onlinelibrary.wiley.com/doi/10.1029/2023JB028090 by University Of Leeds The Brotherton Library, Wiley Online Library on [10/01/2024]. See the Terms and Conditions (https://onlinelibrary.wiley.com/terms-and-conditions) on Wiley Online Library for rules of use; OA articles are governed by the applicable Creative Commons License

McAdoo, D. C., Caldwell, J. G., & Turcotte, D. L. (1978). On the elastic-perfectly plastic bending of the lithosphere under generalized loading with application to the Kurd Trench. *Geophysical Journal of the Royal Astronomical Society*, *54*(1), 11–26. https://doi.org/10.1111/j.1365-246x.1978.tb06753.x

McKenzie, D., & Fairhead, D. (1997). Estimates of the effective elastic thickness of the continental lithosphere from Bouguer and free air gravity anomalies. *Journal of Geophysical Research*, *102*(B12), 27523–27552. https://doi.org/10.1029/97jb02481

McKenzie, D., Jackson, J., & Priestley, K. (2005). Thermal structure of oceanic and continental lithosphere. *Earth and Planetary Science Letters*, *233*(3), 337–349. https://doi.org/10.1016/j.epsl.2005.02.005

Mei, S., Suzuki, A. M., Kohlstedt, D. L., Dixon, N. A., & Durham, W. B. (2010). Experimental constraints on the strength of the lithospheric mantle. *Journal of Geophysical Research*, *115*(B8), B08204. https://doi.org/10.1029/2009jb006873

Molnar, P., & Lyon-Caen, H. (1988). Some simple physical aspects of the support, structure, and evolution of mountain belts. In *Geological society of America special papers* (Vol. 218, pp. 179–208). Geological Society of America. https://doi.org/10.1130/spe218-p179

Monsalve, G., McGovern, P., & Sheehan, A. (2009). Mantle fault zones beneath the Himalayan collision: Flexure of the continental lithosphere. *Tectonophysics*, *477*(1–2), 66–76. https://doi.org/10.1016/j.tecto.2008.12.014

Morelli, C., & Nicolich, R. (1990). A cross section of the lithosphere along the European Geotraverse southern Segment (from the Alps to Tunisia). *Tectonophysics*, *176*(1–2), 229–243. https://doi.org/10.1016/0040-1951(90)90268-d

Priestley, K., Jackson, J. A., & Mckenzie, D. (2008). Lithospheric structure and deep earthquakes beneath India, the Himalaya and southern Tibet. *Geophysical Journal International*, *172*(1), 345–362. https://doi.org/10.1111/j.1365-246x.2007.03636.x

Priestley, K., & McKenzie, D. (2013). The relationship between shear wave velocity, temperature, attenuation and viscosity in the shallow part of the mantle. *Earth and Planetary Science Letters*, *381*, 78–91. https://doi.org/10.1016/j.epsl.2013.08.022

Schulte-Pelkum, V., Monsalve, G., Sheehan, A. F., Shearer, P., Wu, F., & Rajaure, S. (2019). Mantle earthquakes in the Himalayan collision zone. *Geology*, *47*(9), 815–819. https://doi.org/10.1130/g46378.1

Shako, R., Forste, C., Abrikosov, O., Bruinsma, S., Marty, J.-C., Lemoine, J.-M., et al. (2014). Observation of the system Earth from space - CHAMP, GRACE, GOCE and future missions. EIGEN-6C: A high-resolution global gravity combination model including GOCE data. (pp. 155–161). https://doi.org/10.1007/978-3-642-32135-1_20

Turcotte, D. L., & Schubert, G. (2002). *Geodynamics*. Cambridge University Press.

Underdown, R., & Redfern, J. (2008). Petroleum generation and migration in the Ghadames Basin, North Africa: A two-dimensional basin-modeling study. *American Association of Petroleum Geologists Bulletin*, *92*(1), 53–76. https://doi.org/10.1306/08130706032

Watts, A., Lamb, S., Fairhead, J., & Dewey, J. (1995). Lithospheric flexure and bending of the central Andes. *Earth and Planetary Science Letters*, *134*(1–2), 9–21. https://doi.org/10.1016/0012-821x(95)00095-t

Watts, A. B., & Burov, E. B. (2003). Lithospheric strength and its relationship to the elastic and seismogenic layer thickness. *Earth and Planetary Science Letters*, *213*(1–2), 113–131. https://doi.org/10.1016/s0012-821x(03)00289-9

Weston, J., Engdahl, E. R., Harris, J., Di Giacomo, D., & Storchak, D. A. (2018). ISC-EHB: Reconstruction of a robust earthquake data set. *Geophysical Journal International*, *214*(1), 474–484. https://doi.org/10.1093/gji/ggy155

Wimpenny, S. (2022). Weak, seismogenic faults Inherited from Mesozoic rifts control mountain building in the Andean foreland. *Geochemistry, Geophysics, Geosystems*, *23*(3), 1–19. https://doi.org/10.1029/2021gc010270

Wimpenny, S. (2023). Lower-crustal normal faulting and lithosphere rheology in the Atlas Foreland [Software]. Zenodo. https://doi.org/10.5281/zenodo.10262403

Wimpenny, S., & Watson, C. S. (2020). gWFM: A global catalog of moderate-magnitude earthquakes studied using teleseismic body waves. *Seismological Research Letters*, *92*(1), 212–226. https://doi.org/10.1785/0220200218

21699356, 2023, 12, Downloaded from https://agupubs.onlinelibrary.wiley.com/doi/10.1029/2023JB028090 by University Of Leeds The Brotherton Library, Wiley Online Library on [10/01/2024]. See the Terms and Conditions (https://onlinelibrary.wiley.com/terms-and-conditions) on Wiley Online Library for rules of use; OA articles are governed by the applicable Creative Commons License